IEEE Access
Multidisciplinary | Rapid Review | Open Access Journal

Received September 2, 2019, accepted September 21, 2019, date of publication September 26, 2019, date of current version October 7, 2019.

Digital Object Identifier 10.1109/ACCESS.2019.2943886

Forecasting Hourly Solar Irradiance Using Hybrid Wavelet Transformation and Elman Model in Smart Grid

XIAOQIAO HUANG[1,2,3], JUNSHENG SHI[2,3], BIXUAN GAO[2], YONGHANG TAI[2,3], ZAIQING CHEN[3], AND JUN ZHANG[2]

[1]Solar Energy Research Institute, Yunnan Normal University, Kunming 650500, China
[2]School of Physics and Electronic Information, Yunnan Normal University, Kunming 650500, China
[3]Yunnan Key Laboratory of Opto-Electronic Information Technology, Kunming 650500, China

Corresponding authors: Junsheng Shi (shi-js@263.net) and Jun Zhang (junzhang@ynnu.edu.cn)

This work was supported by the National Natural Science Foundation of China under Grant 61875171 and Grant 61865015.

ABSTRACT With the integration of photovoltaic (PV) power into an electrical network, the complexity of the grid management is increasing because of intermittent and fluctuation nature of solar energy. Solar irradiance forecasting is essential to facilitate planning and managing electricity generation and distribution in smart grid cyber-physical system (CPS). The performance of existing short-term forecasting methods is far from satisfactory due to a lack of reliable and fast time-frequency model for continuous-time solar irradiance data. To address this problem, this paper proposes a new method, Elman Neural Network (ENN) driven Wavelet Transform (WT-ENN), for hourly solar irradiance forecasting. Firstly, the solar irradiance series was decomposed into a set of constitutive series using wavelet transform. Secondly, the new wavelet coefficients were predicted by ENNs in every sub-series with the best network structure and parameters. Thirdly, Wavelet reconstruction will predict next hour solar irradiance through the aggregation of outputs of the ensemble of ENNs. Finally, the forecasting performance was evaluated using two large real-world solar irradiance datasets. Experiment results show that the new WT–ENN model outperforms a large number of alternative methods and an average forecast skill of 0.7590 over the persistence model. Thus, it is concluded that the proposed approach can significantly improve the forecasting accuracy and reliability.

INDEX TERMS Smart grid, cyber-physical system, solar energy, solar irradiance forecasting, Elman neural network, wavelet transform.

NOMENCLATURE

CPS	cyber-physical system
PV	photovoltaic
ENN	Elman neural network
WT	wavelet transform
CWT	continuous wavelet transform
DWT	discrete wavelet transform
WT-ENN	Elman neural network driven wavelet transform
IoT	internet of things
NWP	numeric weather predictor
AI	artificial intelligence
SVM	support vector machines
BPNN	back propagation neural network
ARMA	auto-regressive moving average
SOM	self-organizing maps
SVR	support vector regression
PSO	particle swarm optimization
LSTM	long short term memory neural network
MLPNN	multilayer perceptron neural network
TB K-means	transformation based K-means algorithm
GHI	global horizontal irradiance
MBE	mean biased error
MAE	mean absolute error
RMSE	root mean square error
nRMSE	normalized root mean square error
R	Pearson correlation coefficient
FS	forecast skill
FE	forecasting error
WCS	wavelet cross spectrum
COI	cone of influence
RNN	Recurrent Neural Network

The associate editor coordinating the review of this manuscript and approving it for publication was Wei Yu.

I. INTRODUCTION

Because of the challenges of climate change, environmental pollution, and energy insecurity, the market penetration of renewable energy sources is growing rapidly. While renewable energy sources such as solar, wind, and geothermal are in abundance, they are much harder to harvest. Larger scale deployments of smart technologies, which represented by Internet of Things (IoT) and Cyber-Physical Systems (CPS) [1], [2], are needed in order to make these energy supplies more reliable and secure. These promoted the progress of smart grid [3]. Power generation is an important component of smart grid, which is becoming more complex because of the integration of photovoltaic (PV) power into an electrical network. The power generated from the PV power plants is related to the solar irradiance falling on the surface. However, the values of solar irradiance are affected by various atmospheric events such as rain and clouds. Rapid fluctuations of solar irradiance may occur in various regions. The range of solar irradiance fluctuations can reach up to hundreds of W/m^2. As more and more solar power is connected to the grid, the sudden power drop caused by the decrease of solar irradiance will adversely reduce the stability and power quality of the local grid, possibly having a domino effect on the adjacent power nodes [4]. This is a dangerous problem in energy management. The power grid needs to be balanced in real-time, and only limited low-cost storage and spinning reserves are generally available. Predicting solar irradiance is essential to facilitate planning and to managing electricity generation and distribution. These are strong motivations for short-term solar energy production forecasting [5].

A number of models have been proposed to forecast solar irradiance, which can be classified into three categories: physical, statistical and hybrid solar forecasting. The physical models describe how much solar irradiance can be collected with physical considerations. They predict the daily or hourly solar irradiance according to the expected weather conditions of a specific day. There are two well-known physical models, numeric weather predictor (NWP) and clarity index. Although these physical models can interpret internal relationships, their complexity hinders further improvement in forecasting. The statistical models predict the solar irradiance by using the historical samples or spatial-temporal samples, which are good at the short-term forecasting. Statistical techniques can be further divided into time series based methods and artificial intelligence (AI) based methods. The time series based methods includes the AutoRegressive (AR), Autoregressive Moving Average (MA), AutoRegressive Integrated Moving Average (ARIMA) methods [6], [7], which have demonstrated reliable performance and fast prediction. The AI based methods, such as the Artificial Neural Networks (ANN) [8]–[12], Hidden Markov Models (HMMs) [13], Fuzzy Logic [14], Wavelet Networks [15], Long Short-Term Memory Networks (LSTM) [16], K-Nearest Neighbors (KNN) and Support Vector Machines (SVM) [17], [18], and deep learning [19], [20], can deal with the nonlinear and complex solar irradiance series.

The hybrid models have gained a lot of attention as they can combine advantages of different models. A basic idea of the model combination in forecasting is to use each model's unique feature to capture different patterns in the data. There are a few typical hybrid methods in the literature. Sharma *et al.* [21] proposed a mixed wavelet neural network (WNN) for short-term solar irradiance forecasting, with initial application in tropical Singapore. A combination of Morlet and Mexican hat wavelets is used as the activation function in the hidden-layer neurons of a feed forward ANN. The experiment results showed that WNN has better prediction skill than other forecasting techniques. Voyant *et al.* [22] presented a hybrid ARMA/ANN model to predict global radiation. This forecast model has been evaluated with the hourly global radiation data collected from five places in Mediterranean area. Mohammadi *et al.* [23] proposed a hybrid model that combines the SVM and the Wavelet Transform (WT) algorithm to predict horizontal global solar radiation. The SVM-WT model has high preciseness and reliability in estimating the global solar radiation on a horizontal surface. Benmouiza and Cheknane [24] forecasted hourly global horizontal solar radiation by combining the k-means algorithm and ANN. The k-means was used to extract useful information through modeling the time series behavior and discovering the patterns in data clusters. Azimi *et al.* [25] developed a hybrid forecasting method that combines a time-series analysis, a novel clustering technique, a new cluster selection algorithm and a multilayer perceptron neural network (MLPNN) for different time horizons. Li *et al.* [26] proposed a prediction model with Empirical Mode Decomposition (EMD) and ANN to predict long-term solar radiation.

As reported in the literature, the accuracy of solar radiation forecasting is still less satisfactory. The root mean square errors (nRMSE) of existing prediction models are about 10%-24% [20]. Moreover, it lacks of the studies concerning fast time-frequency model, which hinders further advancements in this field. In this paper, we proposed a novel WT-ENN approach that hybridizes wavelet transform (WT) and Elman neural network (ENN) to forecast solar irradiance. Firstly, the original solar irradiance data are decomposed into stable wavelet sub-series for prediction modelling. Then the new wavelet coefficients are optimized by ENN in every sub-series. Finally, the solar irradiance date are reconstructed using the prediction model and the new wavelet coefficients. A large number of experiments are conducted on two real-world datasets to evaluate the performance of the proposed hybrid approach. The experiment results show that the proposed WT-ENN model has superior performance and can effectively improve the prediction accuracy. These also indicate that the accurate forecasting hourly solar irradiance using only historical irradiance without other meteorological parameters is possible.

The novelty of this study is to model the solar irradiance time series, both in temporal and spectral domains. A WT is performed that decompose the irradiance into different frequency and time resolutions, and different ENNs are trained accordingly. The main contributions of this study are as follows:

1) This study improves the performance of ENN models by using WT for the original data and, subsequently, develops an improved WT-ANN hybrid model for solar irradiance forecasting.
2) This study explores the suitability of wavelet-coupled ENN models for the first time in two regions which have abundant solar energy resources.

The organization of the paper is as follows. Section II provides the information about the real-world datasets. The new prediction approach is proposed in Section III. The experiments and results and are reported in Section IV. Finally, conclusions are given in Section V.

II. DATA AND ANALYSIS

In this work, measured global horizontal irradiance (GHI) taken from a meteorological ground station are used to forecast GHI for the next hour. We need to apply lots of real-world data to train and optimize the proposed model. Two real-world datasets are used to evaluate hourly-ahead forecasts of the GHI at the Earth's surface: Kunming (24°51′ N, 102°51′ E, Yunnan, China) and Denver (39°44'N, 105°11'W, Colorado, USA), which have abundant solar energy resources.

Kunming, located at the southwest of China, has a humid subtropical mild summer climate that is mild with dry winters, mild rainy summers and moderate seasonality. The annual average temperature in Kunming is 14.6°C. The altitude is 1895 m. The average sunshine per year is 2172 hours and the annual solar irradiance is about 5500 MJ/m^2. The atmosphere in Kunming is relatively thin, which makes the solar irradiance on the horizontal surface abundant and uniform throughout the year. The Kunming dataset is provided by a portable automatic weather station, which is installed at Yunnan Normal University. The solar irradiance value in this paper refers to the GHI at the Earth's surface. The solar irradiance data and the meteorological data, such as ambient temperature, relative humidity, wind velocity, atmospheric pressure, rainfall and so on, were measured and logged by a data logger (CR1000) every minute during the period from April 12th 2017 to May 29th 2018. We analyze 554,400 data instances (385 days, from April 12th, 2017 to May 29th, 2018,). The first 436,320 data instances, which were produced in 303 days, from April 12th, 2017 to February 9th, 2018, were assigned as a training set for model training and optimization. The remaining 118,080 data instances covering 82 days, from March 8th, 2018 to May 29th, 2018, were assigned as a testing set to evaluate the performance of the forecasting model. Both the training and testing sets include the diverse conditions of weather and cloud content. The data for between February 9th, 2018 and March 8th, 2018 is lost because of the Winter Holiday in China. In this paper, we consider hourly solar irradiance and the data per minute is converted into the data per hour by the average value.

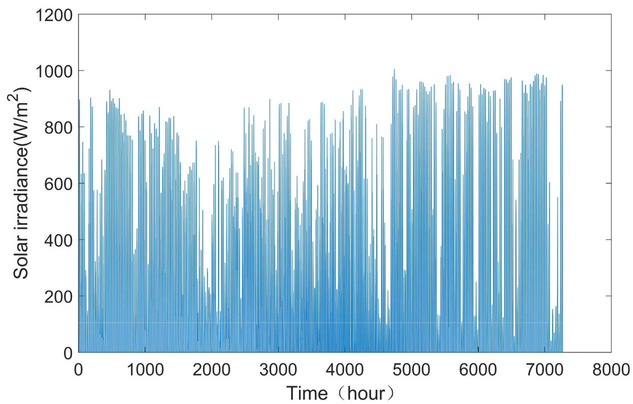

FIGURE 1. Experimental hourly solar irradiance (Training data) recorded by the data logger at Yunnan Normal University in China during period April 12th, 2017–February 9th, 2018.

The measured values of solar irradiance used for training are shown in Figure 1.

Denver, Colorado has a humid subtropical climate that is mild with no dry season, constantly moist (year-round rainfall). Summers are hot and muggy with thunderstorms. Winters are mild with precipitation from mid-latitude cyclones. Seasonality is moderate. The annual average temperature in Denver is 10.1°C, the altitude is 1612 m, the average sunshine per year is 3115 hours and the annual solar irradiance is about 6300 MJ/m^2. The solar irradiance data and the meteorological data are collected every hour during the period from January 1st 2015 to December 30th 2018 by National Renewable Energy Laboratory (NREL). We divide the data into the training, validation and testing data sets, which covers 731(the first two years data), 365 (the third year data) and 365 (the fourth year data) days, respectively.

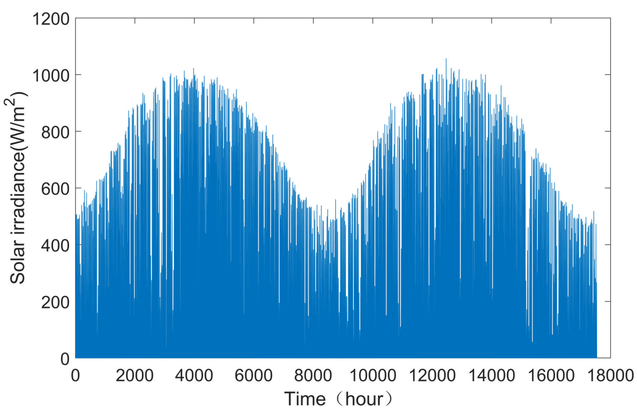

FIGURE 2. Hourly solar irradiance (Training data) at Denver in USA during period January 1st 2015 to December 30th 2016.

The data of solar irradiance for training are shown in Figure 2. Figure 2 and Figure 3 display a clear seasonal component in almost all the plots.

In addition, we study the most important parameters for solar irradiation prediction in this paper. This analysis is done

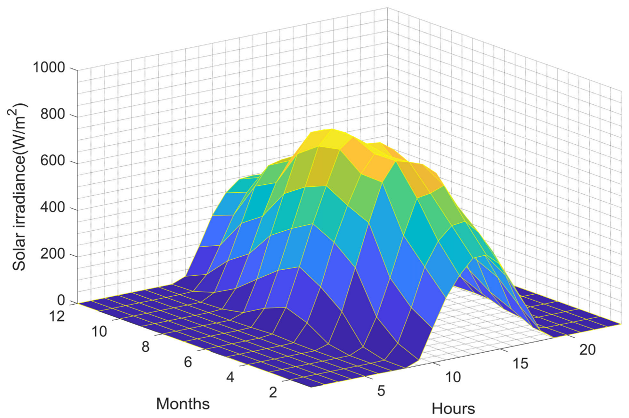

FIGURE 3. Hourly average solar irradiance with different months for training data in Denver.

TABLE 1. Pearson R correlation coefficients between meteorological parameters and solar irradiation in kunming and denver

Meteorological parameters	Pearson R correlation coefficients	
	Kunming	Denver
Wind direction	0.2874	0.0453
Wind speed	0.2444	-0.0858
Atmospheric pressure	0.0124	0.0305
Relative air humidity	-0.5249	-0.3905
Air temperature	0.2247	0.4625
Rainfall	-0.0864	-0.0537

using the data analysis tool for Pearson correlation. Correlation analysis is to check if there is a true relationship between two different variables. The relationships among irradiation and wind direction, wind speed, atmospheric pressure, air temperature, relative air humidity, and rainfall are analyzed to determine which variables are important to prediction. Table 1 shows the results of the correlation analysis on these variables. It can be seen that these parameters have little to no collinearity. Different degrees of correlation occur in different datasets. In this paper, we use only irradiance data and don't consider other meteorological parameters.

III. NEW WT-ENN APPROACH

The proposed approach is a new aggregation of WT representation and ENN neural model. The WT can decompose the original solar irradiance data into a set of better-behaved constitutive sub-series. The future values of these constitutive series are forecasted by the ENN neural model. The ENN model with the inverse WT can predict the future behavior of the solar irradiance.

A. WAVELET IRRADIANCE REPRESENTATION

The wavelet transform is a mathematical approach. It gives the time-frequency representation of a signal with the possibility to adjust the time-frequency resolution. WT can be regarded as the time-frequency analysis method with an adjustable window. In this paper, the solar irradiance series are transformed into a set of constitutive series through

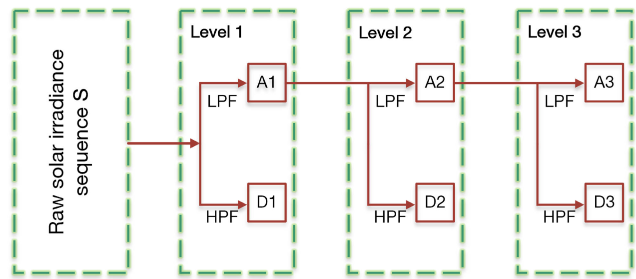

FIGURE 4. Decomposition process of the WT.

wavelet transform. The constitutive series are able to characterize the behind pattern better than the original solar irradiance series.

There are two types of wavelet transform, continuous wavelet transform (CWT) and discrete wavelet transform (DWT). The accuracy of DWT is almost the same as the CWT, but it is more effective in reducing the substantial redundant information generated by the CWT [27].

The CWT $W(a, b)$ of solar irradiance signal $s(t)$ can be defined as

$$\mathrm{W}(a, b) = \frac{1}{\sqrt{a}} \int_{-\infty}^{+\infty} s(t)\, \varphi^{*}\left(\frac{t-b}{a}\right) dt \tag{1}$$

where φ is so-called mother wavelet, φ^{*} is a complex conjugate of φ, the parameter "a" denotes wavelet dilation and controls the spread of the wavelet, parameter "b" denotes time shift of wavelet and determines the central position.

The wavelet transform procedure can be carried out by considering a finite number of positions and resolution levels. In DWT, the decomposition coefficients of the wavelet transform of the hourly solar irradiance are given by

$$\mathrm{W}(\mathrm{m}, \mathrm{n}) = 2^{-(m/2)} \sum_{t=0}^{T-1} s_t \varphi^{*}\left(\frac{t-n \cdot 2^{m}}{2^{m}}\right) \tag{2}$$

where $\varphi^{*}(\cdot)$ is a complex conjugate of the selected wavelet function, s_t is the value of the solar irradiance at hour t, T is the length of the series, W(m, n) is the decomposition coefficient corresponding to position n and resolution level m. The parameters of scaling and translation are functions of the integer variables m and n($a = 2^{m}$, $b = n2^{m}$).

Our new approach is based on Mallat's theory [28] about decomposition and reconstruction for the multiresolution signal. The solar irradiance series are decomposed into the "approximations" and "details". An approximation (A) is the low-frequency representation of the original solar irradiance signal, which maintains the general trend of the original solar irradiance signal; whereas details (D) describe the high-frequency component, which is the difference between two successive approximations. A one-dimensional multilevel (3-level) decomposition process is described in Figure 4. It can be formulated as $f = A3 + D3 + D2 + D1$.

In this paper, according to the relevant research [23], [29], we use Daubechies wavelet of order 5 (abbreviated as DB5)

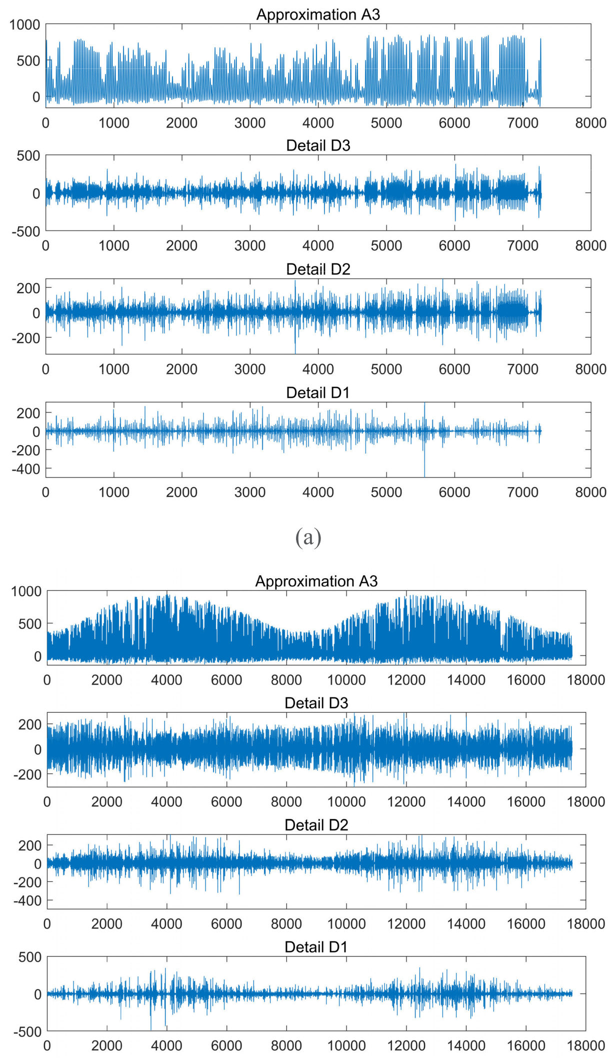

(a)

(b)

FIGURE 5. **Discrete wavelet coefficients (DWC) of the solar irradiation sequence for the WT-ENN model development with approximation (A3) and three levels of detail (D1, D2, and D3) in training period. (a) Kunming, (b) Denver.**

as the mother wavelet $\varphi(t)$ and select three-level decomposition. Figure 5 shows the wavelet decomposed sequences of the solar irradiation.

B. ELMAN NEURAL MODEL

Elman neural network is partially recurrent network or simple recurrent network, which can feedback connections from the hidden layer to its input by an additional context layer [30]–[32]. The context units make the Elman neural networks very sensitive to the historical inputs and qualified for the efficiency in the dynamic signal modeling. The ENN architecture is shown in Figure 6.

The output of an Elman network is described by Equation (1), (2) and (3):

$$y(k) = g(w_3 x(k)) \tag{3}$$

$$x(k) = f(\omega_1 x_c(k) + \omega_2 u(k-1)) \tag{4}$$

$$x_c(k) = x(k-1) \tag{5}$$

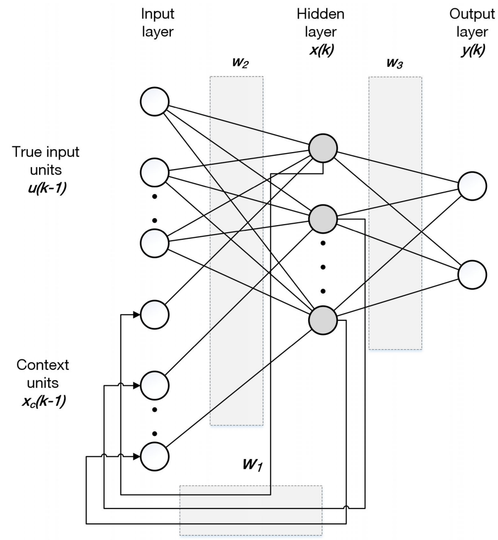

FIGURE 6. **Elman recurrent neural network architecture.**

where, $u(k-1)$ and $y(k)$ are the input and output of the Elman network, respectively, at a discrete time k; $x_c(k)$ is the node of the context layer, $x(k)$ is the node of the hidden layer; and $\omega_1, \omega_2, \omega_3$ are the weight matrices for the context-hidden, input-hidden, and the hidden-output layer, respectively.

In this architecture, the input layer consists of two parts: the true input unit ($u(k-1)$) and the context unit ($x_c(k)$). The context unit only saves the output of the hidden unit in the previous step ($x(k-1)$). Therefore, the network can integrate temporal information tracing back to its initial state.

C. WAVELET ELMAN PREDICTION

The new Algorithm WT-ENN shows the detailed process of our new prediction approach.

The procedure can be described step by step in Figure 7, wavelet transform is implemented in the first and last stages. The actual irradiance time-series are first decomposed into sub-series. The decompose signals are then fed into the ENN at the second stage to predict the future time-series patterns for each of the sub-series. Finally, the solar irradiance date was reconstructed using these new wavelet coefficients.

Step 1: Divide the available data into training, validation and test set.

Step 2: Using the WT algorithm to decompose the original training/validation/test set into the "approximations A3" and "details D1 D2 D3" (3-level decomposition). The purposed of this step is to decrease the non-stationary of the detailed components.

Step 3: Select architecture and training parameters, such as the number of neuron of the hidden layer, layer-delays, train-function, and other training parameters of ENN.

Step 4: Train the model using the training set ("approximations A3").

Step 5: Evaluate the model using the validation set.

Step 6: Repeat steps 3 to 5 using different training parameters.

Algorithm 1 WT-ENN

Input: $X_1, X_2, X_3, \cdots, X_n$, while n is the number of samples.
Output: $Y_1, Y_2, Y_{3,} \cdots, Y_n$.
Procedure:
1. Using WT algorithm to decompose the data of original irradiance time series into the "approximations A3" and "details D1 D2 D3" (four sub-series). Then, these values are described by $x_1, x_2, x_3, \ldots, x_i, \ldots, x_n$ respectively.
2. Each of sub-series A3 D1 D2 D3 are normalized to $[-1, 1]$ using Eq. (6).
3. **Repeat**
4. **For** each sub-series **do**
5. Real-input/output S $= \{(x_i, y_i)\}_{i=1}^{n}$, while $x_i = x_{t-23}, x_{t-22}, \cdots, x_{t-1}, x_t, y_i = x_{t+1}$.
6. **End**
7. **Repeat**
8. **For** each S in the sub-series **do**
9. Initialize ENN structure and parameters. Set the number of neuron of the hidden layer (initial value $= 10$),layer-delays (initial value $= 1{:}1$), train-function (gradient descent with Momentum and Adaptive LR) and Learning Algorithm (Levenberg-Marquardt).
10. Train and optimize the ENN network.
11. Evaluate the network using the validation set.
12. Save the best network.
13. **End for**
14. **Until** maximum number of iterations or stopping criteria is attained.
15. **Repeat**
16. **For** each input in the sub-series (for test samples) **do**
17. Forecast the new wavelet coefficients using the corresponding network and renormalize the data.
18. **End**
19. Calculate the predicted solar irradiance by wavelet reconstruction.

Step 7: Select the best parameters, train data from the training and validation set, and save the best net.

Step 8: Compute this final model using the test set ("approximations A3"), and forecast wavelet coefficients (for each layer).

Step 9: Repeat steps 3 to 8 with the set details D1, D2 and D3.

Step 10: Forecast solar irradiance by wavelet reconstruction. $f = A3 + D3 + D2 + D1$, where, A3', D3', D2' and D1' are the new wavelet coefficients using ENN.

We use Python and Matlab R2016b to develop the experiment program for WT-ENN.

Before applying the training algorithm, the data (input/output) should be normalized to [-1, 1] according to Eq. (6).

$$y = \frac{(y_{max} - y_{min})(x - x_{min})}{(x_{max} - x_{min})} + y_{min} \tag{6}$$

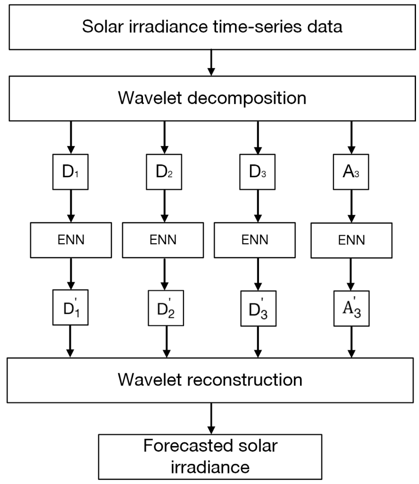

FIGURE 7. The scheme of the WT-ENN forecast model.

where $x \in [x_{min}, x_{max}]$, $y \in [y_{min}, y_{max}]$. "x" is the original datum and "y" is standardized value. We assume that $y_{min} = -1$, $y_{max} = 1$.

IV. EXPERIMENTS AND RESULTS

This section reports a large number of experiments and results on two real-world datasets for performance evaluation.

A. PERFORMANCE METRICS

We use five statistical metrics to assess the performance of the models.

Mean biased error (MBE)

$$MBE = \frac{1}{N} \sum\nolimits_{i=1}^{N} \left(\hat{Y}_i - Y_i\right) \tag{7}$$

where the N is the number of testing instances, $\hat{Y}_i$ is the prediction of the models and Y_i is the measured irradiance mean.

Mean absolute error (MAE)

$$MAE = \frac{1}{N} \sum\nolimits_{i=1}^{N} \left|Y_i - \hat{Y}_i\right| \tag{8}$$

Root mean square error (RMSE)

$$RMSE = \sqrt{\frac{1}{N} \sum\nolimits_{i=1}^{N} \left(\hat{Y}_i - Y_i\right)^2} \tag{9}$$

Normalized root mean square error (nRMSE)

$$nRMSE = \frac{RMSE}{\bar{Y}} \tag{10}$$

where $\bar{Y}$ is the mean value of Y_i.

Furthermore, forecast skill (FS) is a metric to compare a specific model to a reference model (usually persistence), independent of forecast horizon, location or method [33]. It is neutral and useful error metric in solar irradiance forecasting, as given by Eq.(11).

$$\text{FS} = 1 - \frac{nRMSE}{nRMSE_{persistence}} \tag{11}$$

The persistence model is a considerably elementary forecasting model, which is commonly used to justify the performance of the other forecasting models. In this model, the forecasted GHIs is assumed to remain the same with the previous hour.

B. NEURAL NETWORK ARCHITECTURE

The input of ENN is a vector of 24 dimensions, which represents the irradiance values with 1-hour intervals for the previous 24 hours. The single output of ENN is the predicted irradiation value. In order to achieve better network performance, different numbers of hidden neurons and delays are studies for selecting best architecture. A summary of the designed network is given in Table 2.

TABLE 2. Summary of ENN design and architecture Units for Magnetic Properties.

Type	Description
Inputs	0-24h – the component of solar irradiance
Output	t+1h - the component of solar irradiance
Number of Layers	3 - input, hidden, output
Number of Hidden Neurons	15
Number of Delays	1:2
Training Algorithm	gradient descent with Momentum and Adaptive LR
Learning Algorithm	Levenberg-Marquardt

C. FORECASTING RESULTS AND ANALYSIS

The forecasted results are reported in Figure 8 and Table 3. As one can see in Figure 8(a)(b), the blue circle (◯) represents the measured value and the red asterisk ($*$) represents the forecasted value. The trend of the prediction line follows the actual line at every moment. The local enlarged drawing can show the small difference between measured and forecasted values. The forecasted values of solar irradiance well match the groud-truth values. As shown in Figure 8(c)(d), there is a good correlation between the forecasted value and the actual value.

Table 3 and Table 4 report the research on prediction accuracy and the statistical parameters such as RMSE, nRMSE, MBE. Refer to column 4 of Table 3, one can see that the RMSE is 26.84 W/m^2, the nRMSE is 12.37%, the MBE is 0.987 W/m^2, the MAE is 19.33 W/m^2, the Pearson correlation coefficient is 0.9959, and the FS is 0.7718. These are forecasting performance on the Kunming data.

In Denver dataset, it can be seen from column 4 of Table 4 that the RMSE is 25.83 W/m^2, the nRMSE is 14.17%, the mean bias error (MBE) is -0.314 W/m^2, the MAE is 18.24 W/m^2, the Pearson correlation coefficient is 0.9951, and the FS is 0.7590. The experimental results on the two different datasets are very similar. These evaluation results confirm that the proposed WT-ENN approach works very well.

TABLE 3. The performance of WT-ENN and classical Elman (non-wavelet) model in test samples (kunming) measured by Root mean square error (RMSE, W/m^2), nRMSE (%), Mean biased error (MBE, W/m^2), Mean absolute error (MAE, W/m^2), Pearson correlation coefficient (R), and forecast skill (FS).

	ENN		WT-ENN	
	0-24h	8-20h	0-24h	8-20h
RMSE (W/m^2)	68.96	93.09	26.84	30.98
nRMSE (%)	31.77	23.25	12.37	7.74
MBE(W/m^2)	-5.272	-2.102	0.987	-1.173
MAE(W/m^2)	37.33	61.95	19.33	21.73
R(Pearson correlation)	0.9725	0.9500	0.9959	0.9946
FS (forecast skill)	0.4139	0.4176	0.7718	0.8061

TABLE 4. The performance of WT-ENN and classical Elman (non-wavelet) model in test samples (denver).

	ENN		WT-ENN	
	0-24h	8-20h	0-24h	8-20h
RMSE (W/m^2)	73.09	98.49	25.83	32.52
nRMSE (%)	38.79	28.47	14.17	9.40
MBE(W/m^2)	-0.318	-1.228	-0.314	1.850
MAE(W/m^2)	39.32	64.13	18.24	22.54
R(Pearson correlation)	0.9630	0.9387	0.9951	0.9935
FS (forecast skill)	0.3308	0.3326	0.7590	0.7796

Since the solar irradiance is zero or close to zero during the 0-7h and 20-24h, the forecasted values of 8-20h are extracted from 0-24h. As shown from column 5 of Table 3 and 4 that the nRMSE reduces to 7.74% and 9.40% respectively. The local enlarged drawing of Figure 8 suggests, when the actual value of irradiance is 0, there is a certain deviation in the predicted value. In actual forecasting, these meaningless values are usually removed. Overall, these results indicate that the proposed prediction model has excellent performance.

Meanwhile, we conduct a comparison between the proposed hybrid WT-ENN model and the classical ENN model. The results are reported in Table 3 and 4. RMSE decreases from 68.96 to 26.84 W/m^2 (from 73.09 to 26.99 W/m^2 in Denver) when using the hybrid method. The accuracy has been improved by 2.5 times. The performance improvements on other statistical parameters are also significant. It can be inferred from Table 3 and 4 that the proposed hybrid method is effective and its accuracy is outstanding.

The statistical metrics deduced over the test period (Table 3 and 4) exemplifies good predictive skill of the WT-ENN compared to the classical ENN model. It is also of interest to check the time-series of model forecasting for analyzing the hour-to-hour solar irradiance forecasting.

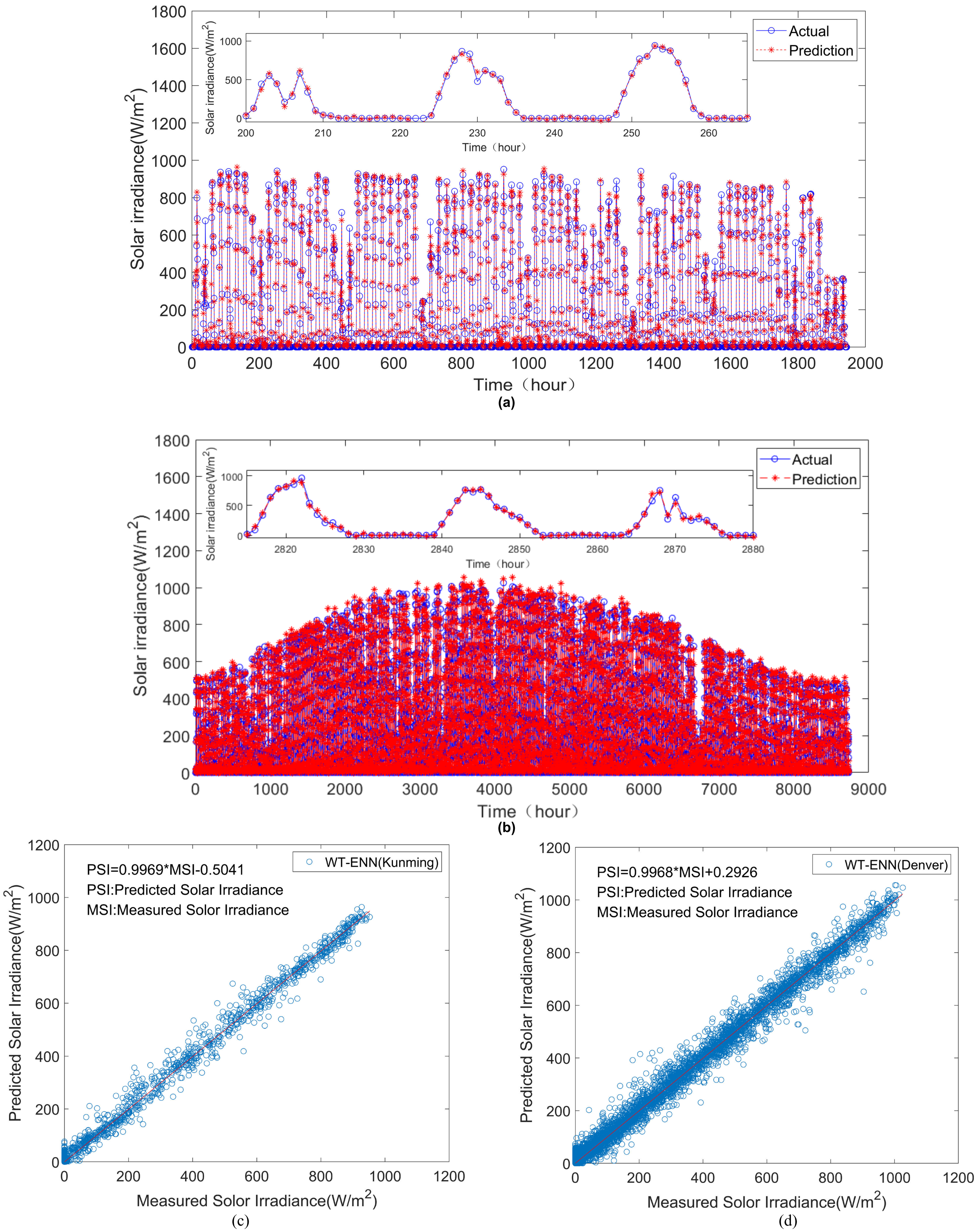

FIGURE 8. Scatter plot of the measured and forecasted hourly solar irradiance. (a)(c) for Kunming; (b)(d) for Denver.

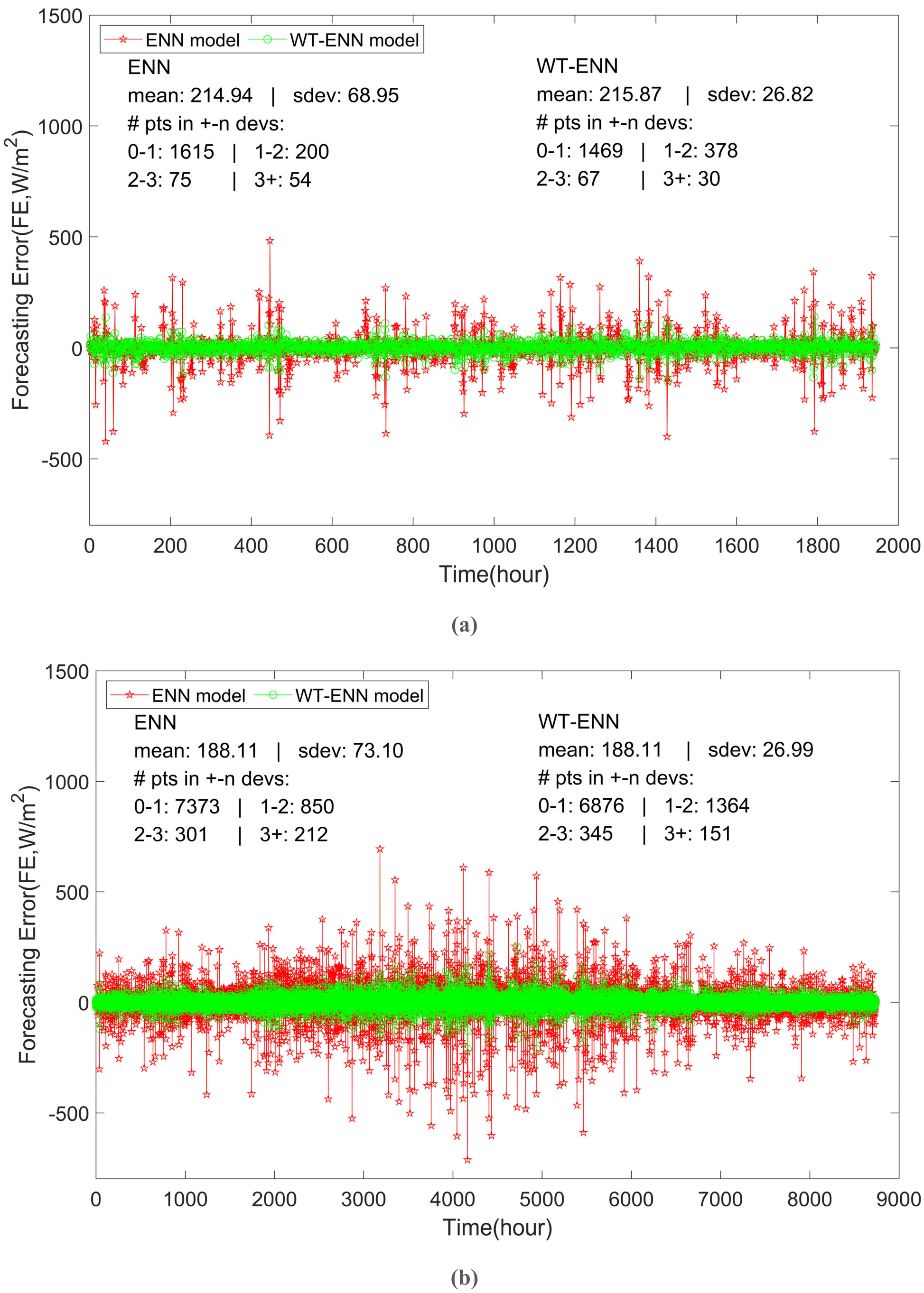

FIGURE 9. **The forecasting error (Forecasting error, FE = $\hat{Y}_i - Y_i$ (W/m^2) in test period. The statistics of forecasting error are shown including the number of points in ±(1, 2 and 3) standard deviations. (a) Kunming, (b) Denver.**

Figure 9 plots the forecasting error (FE) of a time-series for the classical ENN and WT-ENN model. Forecasting error, FE $= \hat{Y}_i - Y_i$ describes the difference between the hourly measured (Y_i) and the hourly forecasted ($\hat{Y}_i$) solar irradiance. The mean of FE, standard deviation (σ) of FE and a numerical count of the datum points in (0–1), (1–2), (2–3) and (3+)σ have been enumerated. There is strong evidence that the classical ENN model exhibits higher amplitude in the fluctuation in FE. This is also verified by the standard deviation of the model's FE. As it can be seen in Figure 9(a), for Kunming, the standard deviation of the WT-ENN model's FE is 26.82. The standard deviation of the ENN model's FE is 68.95. There is a remarkable difference. Meanwhile, the WT-ENN model has 1469 datum point (75.5%) in $<1\sigma$ range. In Figure 9(b), for Denver, the standard deviation of the WT-ENN model's FE is 26.99. The standard deviation of the ENN model's FE is 73.10. Meanwhile, the WT-ENN model has 6876 datum point (78.7%) in $<1\sigma$ range. The results of

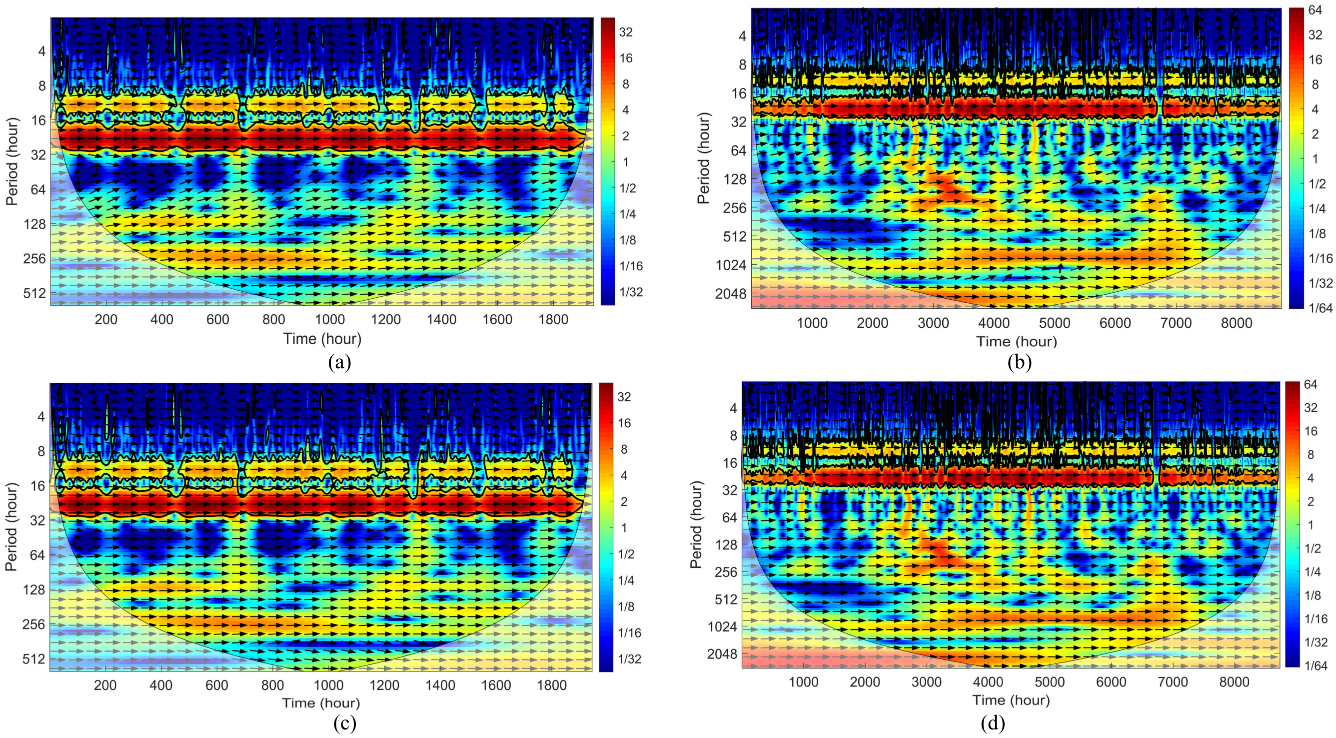

FIGURE 10. Wavelet cross spectrum for measured irradiance and predicated irradiance, where relative phase arrows point right for in-phase and left for anti-phase coherence. (a) ENN approach for Kunming, (b) ENN approach for Denver, (c) WT-ENN approach for Kunming, (d) WT-ENN approach for Denver.

TABLE 5. Comparison of hourly solar irradiance forecasting with some existing methods in the literature.

References	Region	Method	Performance
Emre Akarslan[36]	Antalya, Turkey	Similarity search algorithm	nRMSE=18.67% R=0.9742
Cyril Voyant[22]	Marseille, France	Combining ANN and ARMA	nRMSE= 13.7%
Cyril Voyant[37]	Ajaccio, France	Mix MLP and ARMA with Bayesian rules	nRMSE= 36.59%
R. Azimi[25]	-	TB K-means and MLPNN	RMSE(W/m^2)=29.72 FS=0.6372
Jing Huang[38]	Mildura, Australia	Coupled AutoRegressive and Dynamical System model	nRMSE=16.50%
Emre Akarslan[39]	Afyonkarahisar, Turkey	Multi-dimensional linear prediction filter approach	RMSE(W/m^2)=60.74 nRMSE= 31.29%
Emre Akarslan[40]	Çanakkale, Turkey	Adaptive approaches	nRMSE= 34.86%
Dong Zibo[41], [42]	Colorado, USA	Combining SOM, SVR and PSO	nRMSE= 22%
Mohammad H.[43]	UAE	An improved ANN	rRMSE=9.1%
Lauret, Philippe[44]	Le Raizet, France	ANN, Gaussian, SVM	nRMSE=19.6%
Xiangyun Qing[16]	Island of Santiago, Cape Verde	LSTM	RMSE(W/m^2) =76.245
Present Study	Kunming, China	Proposed WT-ENN approach	nRMSE=12.37% (0-24h; 7.74% for 8-20h) RMSE(W/m^2) =26.84 FS=0.7718
	Denver, USA		nRMSE=14.33% (0-24h; 9.40% for 8-20h) RMSE(W/m^2) =25.83 FS=0.7590

the two regions are similar. All of these results confirm again that the WT-ENN model is more accurate than the classical ENN model.

Figure 10 shows the wavelet cross spectrum (WCS) analysis on two approaches. The bold contour line indicates a 95% confidence level using Monte Carlo simulation with red noise [34]. The power spectrum below the line cone of influence (COI) is uncertain because of edge effects after zero padding. The wavelet spectra reveal high power for the period between 16 and 32 hours, which is marked in oxblood red, implying that it has a significant oscillation with a daily period for solar irradiance. In other words, the irradiance reveals a daily cycle. The area marked in deep blue indicates irregular oscillations.

A WCS plot in Figure 10(a) (b) reveals that in the case of ENN approach, the period between 32 and 128 hours is not correctly modeled. A relative phase difference of 5–95° (direction of small black arrows inside the WCS plot)

TABLE 6. Accuracy results for the proposed forecasting and existing traditional methods as well as the Persistence forecasting method.

Month	Performance Metrics	Methods				
		BPNN	SVM	ENN	**WT-ENN**	Persistence model
Jan.	RMSE (W/m^2)	58.36	71.42	49.42	**18.48**	74.71
	nRMSE (%)	47.81	49.66	46.53	**18.02**	73.59
	Forecast skill	0.3502	0.3252	0.3678	**0.7552**	-
Feb.	RMSE (W/m^2)	64.72	72.66	59.39	**21.63**	91.93
	nRMSE (%)	40.66	41.54	41.86	**15.24**	64.87
	Forecast skill	0.3732	0.596	0.3547	**0.7651**	-
Mar.	RMSE (W/m^2)	68.77	70.73	61.99	**25.14**	112.44
	nRMSE (%)	31.13	31.25	29.84	**11.72**	52.79
	Forecast skill	0.4103	0.4081	0.4347	**0.7781**	-
Apr.	RMSE (W/m^2)	74.76	77.86	74.09	**28.43**	114.46
	nRMSE (%)	32.41	33.14	32.07	**12.07**	48.27
	Forecast skill	0.3285	0.3134	0.3355	**0.7499**	-
May	RMSE (W/m^2)	101.10	100.89	95.74	**35.10**	129.01
	nRMSE (%)	46.00	44.04	41.57	**15.42**	55.97
	Forecast skill	0.1781	0.2132	0.2573	**0.7244**	-
Jun.	RMSE (W/m^2)	112.43	109.29	105.62	**37.03**	144.54
	nRMSE (%)	44.16	41.50	38.34	**13.53**	52.44
	Forecast skill	0.1578	0.2086	0.2688	**0.7418**	-
Jul.	RMSE (W/m^2)	104.09	101.07	99.77	**37.79**	140.28
	nRMSE (%)	40.62	38.29	37.12	**13.87**	51.09
	Forecast skill	0.2050	0.2505	0.2734	**0.7284**	-
Aug.	RMSE (W/m^2)	95.03	95.97	88.20	**30.57**	126.73
	nRMSE (%)	42.29	41.78	37.73	**13.17**	54.46
	Forecast skill	0.2235	0.2328	0.3073	**0.7582**	-
Sep.	RMSE (W/m^2)	71.44	73.89	63.58	**25.01**	112.06
	nRMSE (%)	33.23	33.54	30.51	**11.80**	52.97
	Forecast skill	0.3726	0.3667	0.4240	**0.7772**	-
Oct.	RMSE (W/m^2)	58.81	69.49	52.31	**18.10**	83.03
	nRMSE (%)	39.82	42.57	38.97	**13.68**	63.01
	Forecast skill	0.3681	0.3244	0.3816	**0.7829**	-
Nov.	RMSE (W/m^2)	55.16	68.67	47.38	**17.85**	75.71
	nRMSE (%)	41.85	45.32	41.28	**15.97**	68.07
	Forecast skill	0.3852	0.3342	0.3935	**0.7653**	-
Dec.	RMSE (W/m^2)	49.00	67.67	38.70	**14.88**	67.03
	nRMSE (%)	41.66	48.12	38.84	**15.52**	70.89
	Forecast skill	0.4124	0.3213	0.4521	**0.7811**	-
Average	RMSE (W/m^2)	76.11	81.63	69.68	**25.83**	105.99
	nRMSE (%)	40.14	40.90	37.89	**14.17**	59.04
	Forecast skill	0.3138	0.3048	0.3542	**0.7590**	-

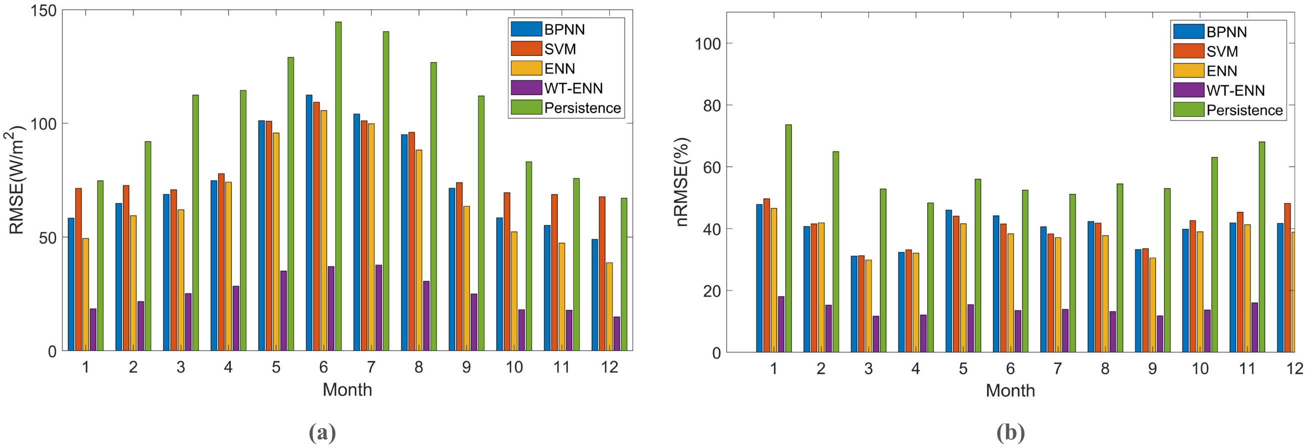

FIGURE 11. Monthly error (RMSE and nRMSE) of prediction for the BPNN, SVM, ENN, WT-ENN and the persistence models in Denver.

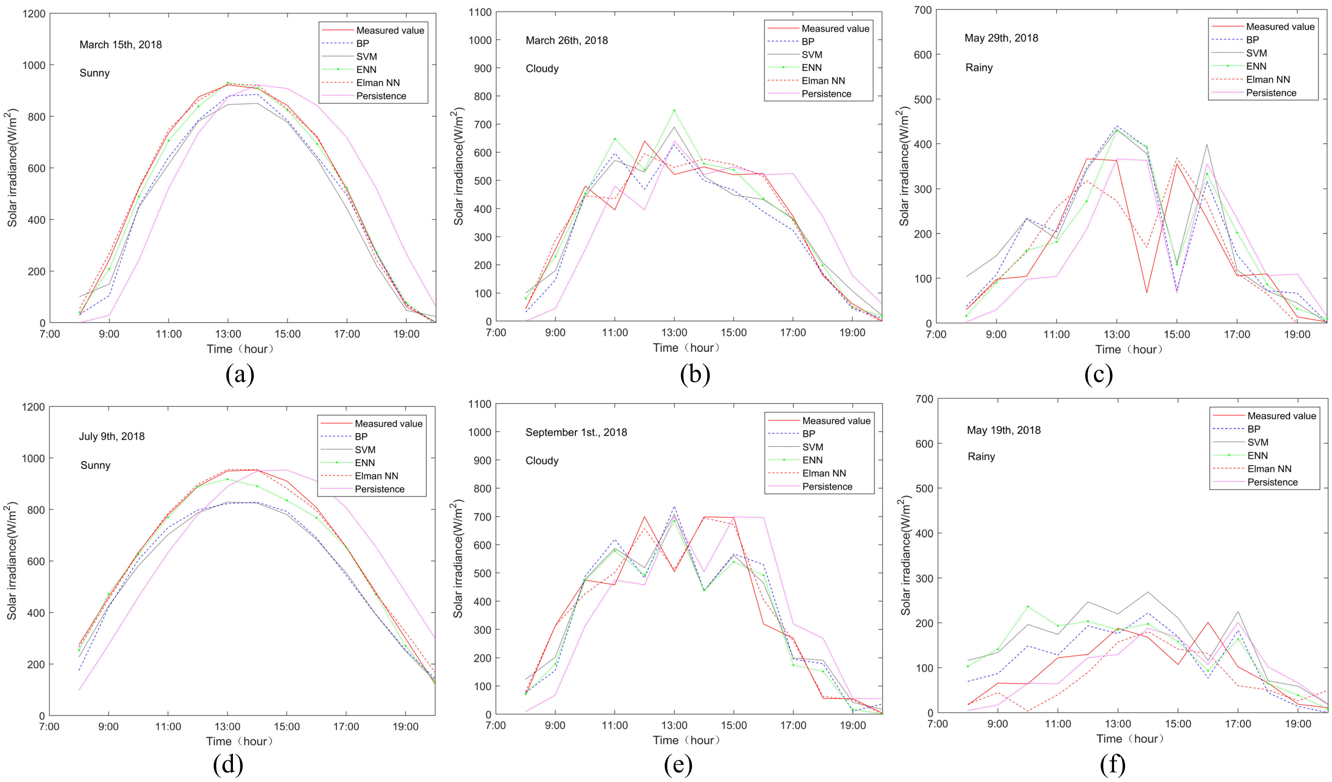

FIGURE 12. Comparison between measured and forecasted hourly solar irradiance for 3 types of weather using different methods. (a) Sunny (March 15th), Kunming, China, (b) Cloudy (March 26th, 2018), Kunming, China, (c) Rainy (May 29th, 2018), Kunming, China, (d) Sunny (July 9th), Denver, USA, (b) Cloudy (September 1st, 2018), Denver, USA, (c) Rainy (May 19rd, 2018), Denver, USA.

between measured and estimated solar irradiance is observed on the time axis. On the other hand, this is not the problem for the WT-ENN approach and the relative phase difference is corrected as shown in Figure 10(c) (d). The direction of small black arrows in the WCS plot is towards right most of the time. This suggests that ENN approach could not well model the frequency contents of the solar irradiance signal related to 32-128 hours. However, when the signal is decomposed, with wavelet decomposition, into relatively simple parts, the problem vanishes.

ENN can use internal memory to exhibit temporal behavior and handle arbitrary input data series, which makes them suitable for time series prediction [35]. When the original solar irradiance datasets are used to as input of ENN, the prediction results are unsatisfactory. Due to the fluctuation nature of solar irradiance, it is difficult to describe the tendency of

TABLE 7. Statistical test between measured and forecasted hourly solar irradiance for a Sunny, Cloudy and Rainy day.

Date	Regions	Weather pattern	Method	RMSE (W/m^2)	nRMSE (%)	MBE (W/m^2)	MAE (W/m^2)	R	Forecast skill
March 15th, 2018	Kunming, China	Sunny	**WT-ENN**	**16.99**	**6.22**	**3.35**	**14.72**	**0.9990**	**0.8597**
			ENN	17.03	6.32	6.91	12.57	0.9992	0.8575
			BPNN	47.16	18.55	22.35	28.71	0.9957	0.5815
			SVM	62.83	23.76	12.13	54.53	0.9938	0.4639
			Persistence	122.57	44.32	0	76.83	0.9407	-
March 26th, 2018	Kunming, China	Cloudy	**WT-ENN**	**24.98**	**13.50**	**3.54**	**19.81**	**0.9949**	**0.7555**
			ENN	76.11	37.65	-13.58	38.35	0.9551	0.3183
			BPNN	70.78	39.84	10.89	40.84	0.9536	0.2787
			SVM	69.90	34.17	-16.03	51.50	0.9561	0.3813
			Persistence	104.13	55.23	0	63.01	0.8995	-
May 29th , 2018	Kunming, China	Rainy	**WT-ENN**	**35.90**	**41.64**	**-0.3903**	**23.42**	**0.9568**	**0.6506**
			ENN	90.22	92.12	-12.09	48.28	0.7602	0.2269
			BPNN	96.11	92.75	-17.78	46.79	0.7440	0.2216
			SVM	96.76	79.40	-36.03	61.65	0.7584	0.3337
			Persistence	102.29	119.16	0	54.83	0.6536	-
July 9th , 2018	Denver, USA	Sunny	**WT-ENN**	**16.40**	**4.75**	**1.20**	**12.65**	**0.9990**	**0.8493**
			ENN	28.71	8.52	9.60	21.20	0.9981	0.7296
			BPNN	68.55	22.63	43.48	49.72	0.9961	0.2821
			SVM	67.32	21.89	38.92	50.87	0.9988	0.3055
			Persistence	109.20	31.52	0	79.41	0.9562	-
September 1st, 2018	Denver, USA	Cloudy	**WT-ENN**	**27.13**	**14.15**	**0.8789**	**18.15**	**0.9943**	**0.7934**
			ENN	102.18	56.71	12.46	64.24	0.9166	0.1720
			BPNN	114.65	57.91	-5.37	79.12	0.8934	0.1546
			SVM	105.45	51.22	-13.24	77.78	0.9114	0.2521
			Persistence	131.93	68.49	0	75.93	0.8648	-
May 19th , 2018	Denver, USA	Rainy	**WT-ENN**	**35.58**	**72.07**	**3.30**	**28.92**	**0.8454**	**0.0182**
			ENN	55.62	73.54	-22.85	35.13	0.7973	-0.002
			BPNN	47.96	65.16	-20.93	35.42	0.8030	0.1123
			SVM	75.23	68.91	-56.50	63.64	0.7869	0.0612
			Persistence	38.67	73.40	0	23.63	0.8281	-

solar irradiance for accurate forecasting. Considering that the irradiance in the same area is mainly affected by the weather, the solar irradiance series can be regarded as a combination of sub-series with different frequencies. Each sub-series corresponds to a frequency range and shows regularity. They can be predicted more accurately than the original data sequence.

D. COMPARISON TO DIFFERENT FORECASTING STRATEGIES

The comparison of hourly solar irradiance forecasting with several existing methods in literature are shown in Table 5. The proposed WT-ENN approach has better prediction accuracy than the other methods. WT-ENN consistently outperforms all other models.

Table 6 reports the accuracy of our WT-ENN method and other models including the BPNN, SVM, ENN and the Persistence forecasting method. The forecast accuracy is calculated for each month and then averaged to provide the performance measures for each month of the year 2018 in Denver region. The details of the monthly errors in every year are provided in Figure 11. The forecasting results indicate that the WT-ENN method outperforms other common neural network techniques and Persistence forecasting method.

Furthermore, three types of weather are chosen to compare the performance of different methods, as shown in Figure 12 and Table 7. In Figure 12 (a) (d)(sunny day, March 15th Kunming, July 9th in Denver). The predicted curves are in reasonably good agreement with measure curves using the proposed method. The nRMSE is only 6.55% and 4.75% respectively, the accuracy of the models using BPNN and SVM methods is similar to that in Denver data set. However, with Kunming data set, there are some differences between them. In Figure 12 (b) (e) (cloudy day, March 26th, in Kunming, September 1st in Denver), there are some differences between the predicted value the actual value.

Compared with the ENN, BPNN and SVM, the performance advantage of WT-ENN is significant. It is relatively difficult to predict the hourly irradiance values of the cloudy day because of the rapid change in hourly weather types during the predicted day. WT-ENN model is excellent. In Figure 12 (c) (rainy day, May 29th, in Kunming), WT-ENN shows big advantage over other methods. In Figure 12 (f) (rainy day, May 19th in Denver), the advantage of WT-ENN is not so significant. All related results are reported in Table 7.

The results show that our WT-ENN method has superior prediction performance in sunny days. It also produces good results for cloudy and rainy days. In WT-ENN, the data is processed by wavelet transform and some fluctuations were filtered out, so the prediction accuracy and reliability can be improved.

V. CONCLUSIONS

In this study, we proposed a new WT-ENN approach, which combines wavelet transform (WT) and Elman neural network (ENN) to forecast hourly solar irradiance in smart grid cyber-physical system. The traditional RNN and ANN approaches lack the ability to capture time-frequency signals. In this paper, the complex solar irradiance signals are decomposed into relatively simple time series with varying time and frequency resolutions using wavelet decomposition. Meanwhile, considering the characteristics of solar irradiance data, ENN modeling, which is the simpler RNN, is applied to these simple time series. Finally, the predicted time series are reconstructed to form an estimate of the final solar irradiance signal. Two real-world datasets with different regions and different types of climate were used for comprehensive performance evaluation. A large number of experiment results show that the proposed WT-ENN approach can significantly improves the forecasting performance. With five different statistical validation metrics, WT-ENN's performance consistently outperforms other comparison models. Our approach can achieve the following best performance. The RMSE is 26.84 W/m^2 and 25.83 W/m^2, the nRMSE is 12.37% and 14.17%, respectively. The forecast skill (over the persistence model) is 0.7718 and 0.7590, respectively. Their results are similar in different regions. The results also indicate that the single variable of historical irradiance could yield accurate forecasting hourly solar irradiance.

REFERENCES

[1] Y. Liu, Y. Peng, B. Wang, S. Yao, and Z. Liu, ''Review on cyber-physical systems,'' *IEEE/CAA J. Autom. Sinica*, vol. 4, no. 1, pp. 27–40, Jan. 2017.

[2] J. Lin, W. Yu, N. Zhang, X. Yang, H. Zhang, and W. Zhao, ''A survey on Internet of things: Architecture, enabling technologies, security and privacy, and applications,'' *IEEE Internet Things J.*, vol. 4, no. 5, pp. 1125–1142, Oct. 2017.

[3] X. Yu and Y. Xue, ''Smart grids: A cyber–physical systems perspective,'' *Proc. IEEE*, vol. 104, no. 5, pp. 1058–1070, May 2016.

[4] Y. Chu, H. T. C. Pedro, and C. F. M. Coimbra, ''Hybrid intra-hour DNI forecasts with sky image processing enhanced by stochastic learning,'' *Sol. Energy*, vol. 98, pp. 592–603, Dec. 2013.

[5] F.-V. Gutierrez-Corea, M. A. Manso-Callejo, M.-P. Moreno-Regidor, and M.-T. Manrique-Sancho, ''Forecasting short-term solar irradiance based on artificial neural networks and data from neighboring meteorological stations,'' *Sol. Energy*, vol. 134, pp. 119–131, Sep. 2016.

[6] L. Mora-López and M. Sidrach-de-Cardona, ''Multiplicative ARMA models to generate hourly series of global irradiation,'' *Sol. Energy*, vol. 63, no. 5, pp. 283–291, 1998.

[7] P. Bacher, H. Madsen, and H. A. Nielsen, ''Online short-term solar power forecasting,'' *Sol. Energy*, vol. 83, no. 10, pp. 1772–1783, 2009.

[8] D. V. S. K. K. Rao, M. Premalatha, and C. Naveen, ''Analysis of different combinations of meteorological parameters in predicting the horizontal global solar radiation with ANN approach: A case study,'' *Renew. Sustain. Energy Rev.*, vol. 91, pp. 248–258, Aug. 2018.

[9] C. Cornaro, M. Pierro, and F. Bucci, ''Master optimization process based on neural networks ensemble for 24-h solar irradiance forecast,'' *Sol. Energy*, vol. 111, pp. 297–312, Jan. 2015.

[10] K. Dahmani, R. Dizene, G. Notton, C. Paoli, C. Voyant, and M. L. Nivet, ''Estimation of 5-min time-step data of tilted solar global irradiation using ANN (Artificial Neural Network) model,'' *Energy*, vol. 70, pp. 374–381, Jun. 2014.

[11] S. Leva, A. Dolara, F. Grimaccia, M. Mussetta, and E. Ogliari, ''Analysis and validation of 24 hours ahead neural network forecasting of photovoltaic output power,'' *Math. Comput. Simul.*, vol. 131, pp. 88–100, Jan. 2017.

[12] B. Amrouche and X. Le Pivert, ''Artificial neural network based daily local forecasting for global solar radiation,'' *Appl. Energy*, vol. 130, pp. 333–341, Oct. 2014.

[13] F. O. Hocaoğlu, ''Stochastic approach for daily solar radiation modeling,'' *Sol. Energy*, vol. 85, no. 2, pp. 278–287, Feb. 2011.

[14] A. Moghaddamnia, R. Remesan, M. H. Kashani, M. Mohammadi, D. Han, and J. Piri, ''Comparison of LLR, MLP, Elman, NNARX and ANFIS Models–with a case study in solar radiation estimation,'' *J. Atmos. Sol.-Terr. Phys.*, vol. 71, nos. 8–9, pp. 975–982, Jun. 2009.

[15] A. Mellit, M. Benghanem, and S. A. Kalogirou, ''An adaptive wavelet-network model for forecasting daily total solar-radiation,'' *Appl. Energy*, vol. 83, no. 7, pp. 705–722, Jul. 2006.

[16] X. Qing and Y. Niu, ''Hourly day-ahead solar irradiance prediction using weather forecasts by LSTM,'' *Energy*, vol. 148, pp. 461–468, Apr. 2018.

[17] R. Meenal and A. I. Selvakumar, ''Assessment of SVM, empirical and ANN based solar radiation prediction models with most influencing input parameters,'' *Renew. Energy*, vol. 121, pp. 324–343, Jun. 2018.

[18] F. Wang, Z. Zhen, B. Wang, and Z. Mi, ''Comparative study on KNN and SVM based weather classification models for day ahead short term solar PV power forecasting,'' *Appl. Sci.*, vol. 8, no. 1, p. 28, Jan. 2018.

[19] K. Kaba, M. Sarigül, M. Avci, and H. M. Kandirmaz, ''Estimation of daily global solar radiation using deep learning model,'' *Energy*, vol. 162, pp. 126–135, 2018.

[20] C. Voyant, G. Notton, S. Kalogirou, M.-L. Nivet, C. Paoli, F. Motte, and A. Fouilloy, ''Machine learning methods for solar radiation forecasting: A review,'' *Renew. Energy*, vol. 105, pp. 569–582, May 2017.

[21] V. Sharma, D. Yang, W. Walsh, and T. Reindl, ''Short term solar irradiance forecasting using a mixed wavelet neural network,'' *Renew. Energy*, vol. 90, pp. 481–492, May 2016.

[22] C. Voyant, M. Muselli, C. Paoli, and M.-L. Nivet, ''Hybrid methodology for hourly global radiation forecasting in Mediterranean area,'' *Renew. Energy*, vol. 53, pp. 1–11, May 2013.

[23] K. Mohammadi, S. Shamshirband, C. W. Tong, M. Arif, D. Petković, and C. Sudheer, ''A new hybrid support vector machine–wavelet transform approach for estimation of horizontal global solar radiation,'' *Energy Convers. Manage.*, vol. 92, pp. 162–171, Mar. 2015.

[24] K. Benmouiza and A. Cheknane, ''Forecasting hourly global solar radiation using hybrid k-means and nonlinear autoregressive neural network models,'' *Energy Convers. Manage.*, vol. 75, pp. 561–569, Nov. 2013.

[25] R. Azimi, M. Ghayekhloo, and M. Ghofrani, ''A hybrid method based on a new clustering technique and multilayer perceptron neural networks for hourly solar radiation forecasting,'' *Energy Convers. Manage.*, vol. 118, pp. 331–344, Jun. 2016.

[26] F.-F. Li, S.-Y. Wang, and J.-H. Wei, ''Long term rolling prediction model for solar radiation combining empirical mode decomposition (EMD) and artificial neural network (ANN) techniques,'' *J. Renew. Sustain. Energy*, vol. 10, no. 1, 2018, Art. no. 013704.

[27] J. P. S. Catalão, H. M. I. Pousinho, and V. M. F. Mendes, ''Hybrid wavelet-PSO-ANFIS approach for short-term electricity prices forecasting,'' *IEEE Trans. Power Syst.*, vol. 26, no. 1, pp. 137–144, Feb. 2011.

[28] S. G. Mallat, ''A theory for multiresolution signal decomposition: The wavelet representation,'' *IEEE Trans. Pattern Anal. Mach. Intell.*, vol. 11, no. 7, pp. 674–693, Jul. 1989.

[29] A. J. Conejo, M. A. Plazas, R. Espinola, and A. B. Molina, "Day-ahead electricity price forecasting using the wavelet transform and ARIMA models," *IEEE Trans. Power Syst.*, vol. 20, no. 2, pp. 1035–1042, May 2005.
[30] J. L. Elman, "Finding tructure in Time," *Cogn. Sci.*, vol. 14, pp. 179–211, 1990.
[31] M. Beccali, M. Cellura, V. Lo Brano, and A. Marvuglia, "Short-term prediction of household electricity consumption: Assessing weather sensitivity in a Mediterranean area," *Renew. Sustain. Energy Rev.*, vol. 12, no. 8, pp. 2040–2065, Oct. 2008.
[32] J.-G. Wu and H. Lundstedt, "Prediction of geomagnetic storms from solar wind data using Elman recurrent neural networks," *Geophys. Res. Lett.*, vol. 23, no. 4, pp. 319–322, 1996.
[33] D. Yang, J. Kleissl, C. A. Gueymard, H. T. C. Pedro, and C. F. M. Coimbra, "History and trends in solar irradiance and PV power forecasting: A preliminary assessment and review using text mining," *Sol. Energy*, vol. 168, pp. 60–101, Jul. 2018.
[34] A. Grinsted, J. C. Moore, and S. Jevrejeva, "Application of the cross wavelet transform and wavelet coherence to geophysical time series," *Nonlinear Processes Geophys.*, vol. 11, nos. 5–6, pp. 561–566, 2004.
[35] J. Wang, W. Zhang, Y. Li, J. Wang, and Z. Dang, "Forecasting wind speed using empirical mode decomposition and Elman neural network," *Appl. Soft Comput.*, vol. 23, pp. 452–459, Oct. 2014.
[36] E. Akarslan and F. O. Hocaoglu, "A novel method based on similarity for hourly solar irradiance forecasting," *Renew. Energy*, vol. 112, pp. 337–346, Nov. 2017.
[37] C. Voyant, C. Darras, M. Muselli, C. Paoli, M.-L. Nivet, and P. Poggi, "Bayesian rules and stochastic models for high accuracy prediction of solar radiation," *Appl. Energy*, vol. 114, pp. 218–226, Feb. 2014.
[38] J. Huang, M. Korolkiewicz, M. Agrawal, and J. Boland, "Forecasting solar radiation on an hourly time scale using a coupled autoregressive and dynamical system (CARDS) model," *Sol. Energy*, vol. 87, pp. 136–149, Jan. 2013.
[39] E. Akarslan, F. O. Hocaoğlu, and R. Edizkan, "A novel M-D (multi-dimensional) linear prediction filter approach for hourly solar radiation forecasting," *Energy*, vol. 73, pp. 978–986, Aug. 2014.
[40] E. Akarslan and F. O. Hocaoglu, "A novel adaptive approach for hourly solar radiation forecasting," *Renew. Energy*, vol. 87, pp. 628–633, Mar. 2016.
[41] Z. Dong, D. Yang, T. Reindl, and W. M. Walsh, "A novel hybrid approach based on self-organizing maps, support vector regression and particle swarm optimization to forecast solar irradiance," *Energy*, vol. 82, pp. 570–577, Mar. 2015.
[42] M. H. Alobaidi, P. R. Marpu, T. B. M. J. Ouarda, and H. Ghedira, "Mapping of the solar irradiance in the UAE using advanced artificial neural network ensemble," *IEEE J. Sel. Topics Appl. Earth Observ. Remote Sens.*, vol. 7, no. 8, pp. 3668–3680, Aug. 2014.
[43] P. Lauret, C. Voyant, T. Soubdhan, M. David, and P. Poggi, "A benchmarking of machine learning techniques for solar radiation forecasting in an insular context," *Sol. Energy*, vol. 112, pp. 446–457, Feb. 2015.

XIAOQIAO HUANG received the M.S. degree in optical engineering from Yunnan Normal University, China, in 2007, where he is currently an Associate Professor with the School of Physics and Electronic Information. His current interests include digital image processing and big data processing technology.

JUNSHENG SHI received the M.S. degree in applied physics from the Hebei University of Technology, in 1994, and the Ph.D. degree in optical engineering from the Beijing Institute of Technology, in 2005.

He is currently a Professor with the School of Physics and Electronic Information, Yunnan Normal University, China. His research interests include color science and engineering, characteristics of the human visual systems and its application for color imaging, and digital image processing.

BIXUAN GAO, photograph and biography not available at the time of publication.

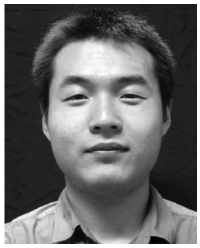

YONGHANG TAI received the M.Sc. degree in optic engineering form Yunnan Normal University, in 2012, and the Ph.D. degree in computer science from Deakin University, Australia, in 2019. His current research interests include physics-based simulation, haptic rendering, and virtual reality. In addition, he focuses on physics-based deformation and virtual surgical simulation.

ZAIQING CHEN received the M.S. degree in computer science from Yunnan University, in 2008, and the Ph.D. degree in photovoltaic engineering from Yunnan Normal University, in 2013, where he is currently an Associate Professor with the Color & Image Vision Lab.

His research interests include 3D displays, color vision, and computer vision.

JUN ZHANG received the Ph.D. degree in computer science from the University of Wollongong, Wollongong, Australia, in 2011. He is currently an Associate Professor with the School of Software and Electrical Engineering and the Deputy Director of the Swinburne Cybersecurity Lab, Swinburne University of Technology, Australia. He has published more than 80 research articles in refereed international journals and conferences, such as the IEEE Communications Surveys and Tutorials (COMST), IEEE/ACM Transactions on Networking (ToN), IEEE Transactions on Image Processing (TIP), IEEE Transactions on Parallel and Distributed Systems (TPDS), IEEE Transactions on Information Forensics and Security (TIFS), *ACM Conference on Computer and Communications Security* (CCS), and *ACM Asia Conference on Computer and Communications Security* (ASIACCS). His research interests include cybersecurity and applied machine learning. He has been internationally recognized as an Active Researcher in cybersecurity, evidenced by his chairing (PC Chair, Workshop Chair, or Publicity Chair) of eight international conferences, since 2013, and presenting invited keynote addresses in two conferences and an invited lecture in IEEE SMC Victorian Chapter.